

The Mechanisms of Tsunami Amplification and the Earthquake Source of the 2021 M7 Acapulco, Mexico, Earthquake

Diego Melgar*¹, Angel Ruiz-Angulo², Brendan W. Crowell³, Eric J. Fielding⁴, & Erica A. Solano-Hernandez⁵

¹*Department of Earth Sciences, University of Oregon, Eugene, OR, USA*

²*Institute of Earth Sciences, University of Iceland, Reykjavik, Iceland*

³*Department of Earth and Space Sciences, University of Washington, Seattle, WA, USA*

⁴*Jet Propulsion Laboratory, Pasadena, CA, USA*

⁵*Universidad del Mar campus Puerto Ángel, Oaxaca, Mexico*

*Corresponding author: dmelgarm@uoregon.edu

This is a non-peer reviewed pre-print submitted to EarthArXiv. This paper has been submitted to the Bulletin of the Seismological Society of America for review.



The Mechanisms of Tsunami Amplification and the Earthquake Source of the 2021 M7 Acapulco, Mexico, Earthquake

Diego Melgar¹, Angel Ruiz-Angulo², Brendan W. Crowell³, Eric J. Fielding⁴, & Erica A. Solano-Hernandez⁵

¹*Department of Earth Sciences, University of Oregon, Eugene, OR, USA*

²*Institute of Earth Sciences, University of Iceland, Reykjavik, Iceland*

³*Department of Earth and Space Sciences, University of Washington, Seattle, WA, USA*

⁴*Jet Propulsion Laboratory, Pasadena, CA, USA*

⁵*Universidad del Mar campus Puerto Ángel, Oaxaca, Mexico*

ABSTRACT

Here we show a slip model for the 2021 M7 Acapulco, Mexico, earthquake produced by inversion of strong motion, GNSS, tide gauge, and InSAR data. The earthquake occurs within the Guerrero gap, identified as a region of concern for its seismogenic potential and paucity of large events. We find that rupture was compact, constrained to depths between 10 and 20 km and consistent of two main slip patches. The slip model leaves a broad swath of the megathrust unbroken. Whether the event signals a reactivation of large earthquakes in the region remains unknown. We find that tide gauge recordings inside Acapulco Bay for the M7 1962 earthquake and the 2021 event are strikingly similar, we interpret this as weak evidence that 2021 is a repeat of 1962. We also produce a high resolution hydrodynamic model of the resulting tsunami using the slip model as initial condition and place special emphasis in understanding the long duration (~17 hr) of waves inside the bay. We find that simple bay resonance alone does not account for the features of the event. Rather it is a complex interaction with shelf modes and edge waves which continuously re-excite the bay resonance that leads to the protracted tsunami disturbances. Furthermore, we find that significant currents in excess of 1 m/s occur in localized portions of the bay even when wave amplitudes remain small.

KEY POINTS

- We analyze the earthquake source and tsunami propagation of the Acapulco earthquake
- We find that the event rupture only a small portion of the Guerrero gap
- We establish that tsunami amplification is due to bay resonance, edge waves, and shelf modes

INTRODUCTION

On September 8th 2021 1:47:47 UTC an $M_w 7.0$ ($M_0 = 3.5 \times 10^{19}$ N-m) earthquake with hypocenter ~5 km offshore the city of Acapulco struck the southern Mexican Pacific coast (Figure 1A). This region of the country is a subduction zone where the Cocos plate subducts beneath North America at ~6 cm/yr with a slightly oblique convergence direction (e.g. Kazachkina et al., 2020). The margin is seismically quite active, with many large ~M7-M8 events in pre- and instrumental times (Castro et al., 2016; Sawires et al., 2019; Suarez et al., 2020). However, the ~250km long part of the megathrust that lies roughly between -101.2° and -99° has been relatively quiet since 1962 when two large ($M_s 6.7$ and $M_s 7.0$, Figure 1) took place in quick succession (Ortiz et al., 2000). For this reason, this part of the subduction system that lies offshore the state of Guerrero is known as the “Guerrero gap”.

The 2021 earthquake is thus important because it signals a potential reactivation of large events in the region. Here we will present a slip inversion calculated from regional strong motion, high-rate global navigation satellite system (HR-GNSS), tide gauge, and interferometric synthetic aperture radar (InSAR, Figure 1). We will show that the slip model for the Acapulco earthquake is quite compact and leaves plenty of the Guerrero gap still unbroken. The event is also of significant interest because it ruptured immediately underneath Acapulco bay (Figures 1A, 1B). Its crustal deformation, both inferred from the InSAR data (Figure 2B) as well as modeled from the slip inversion (Figure 2B) show ~15-20 cm of widespread uplift of the bay. This led to an almost instantaneous tsunami which was recorded by the ACAP tide gauge inside the bay and which also clearly shows ~16cm of uplift (Figure 3A,B).

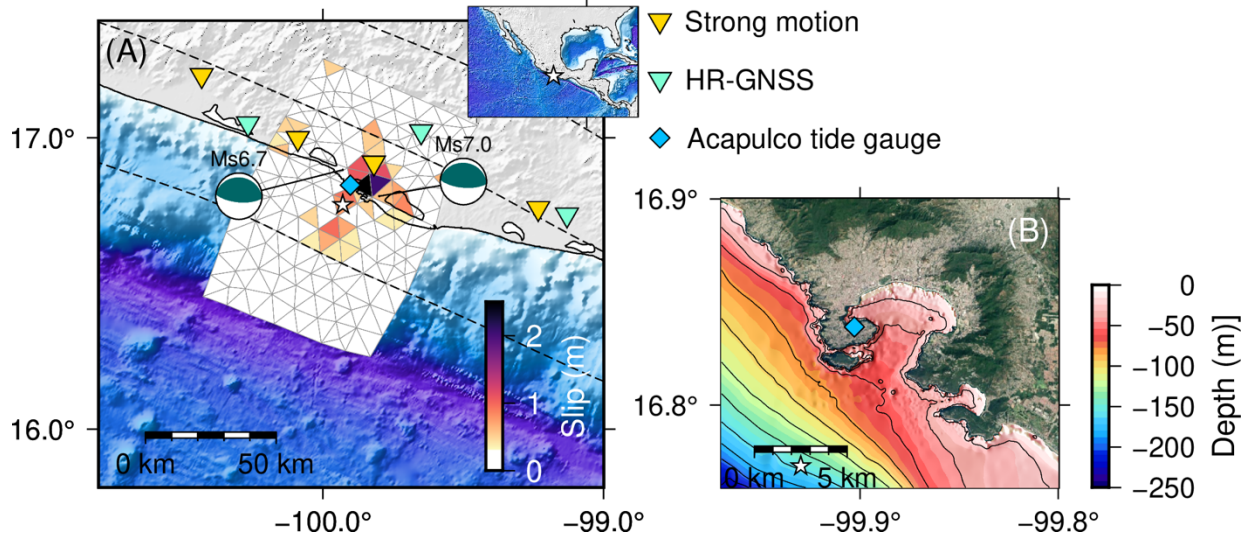


Figure 1. (A) Regional context slip inversion results. Strong motion, GBNSS, and tide gauge stations sued are shown with inverted triangles. Dashed lines are 10 km depth contours from the slab 2 model (Hayes *et al.*, 2018). White star is the hypocenter location from the SSN. Focal mechanisms are for the two events of the 1962 doublet (Ortiz *et al.*, 2000). (B) Close-up of Acapulco bay showing the location for the ACAP tide gauge and bathymetry contoured at 20 m intervals.

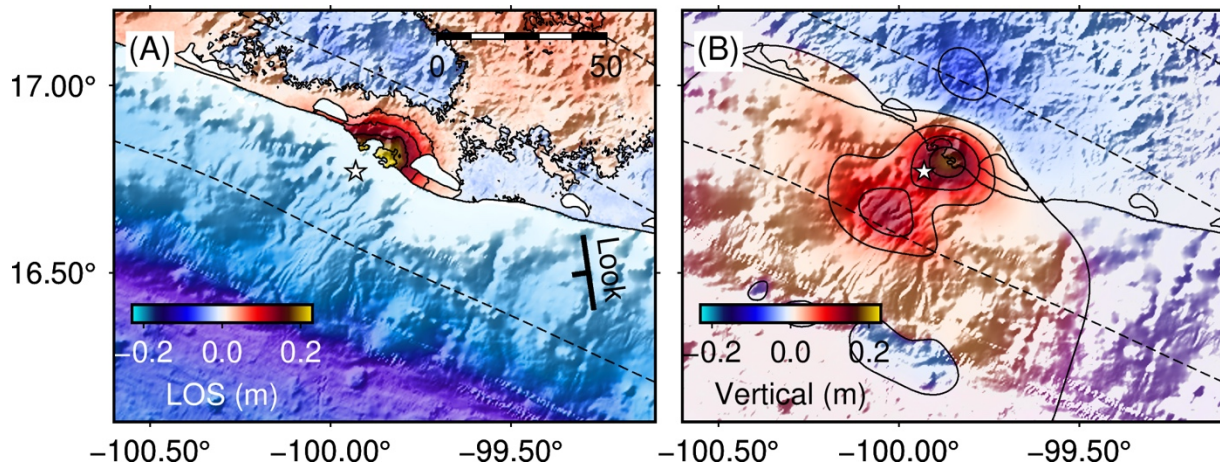


Figure 2. (A) InSAR line of sight deformation from time series analysis. Positive is motion towards the satellite. (B) Predicted vertical deformation from the slip inversion in Figure 1A.

The history of tsunami recordings inside Acapulco bay is extensive (e.g. Sanchez & Farreras, 1993; Geist & Parsons, 2006). As detailed by Zaytsev *et al.* (2016) and Ortiz-Huerta *et al.* (2018) it is well established that far field tsunamis, which have small amplitudes outside the bay, are amplified within it, they have near monochromatic behavior (period ~ 30 min), and can have long durations. However, little is known about how regional events will behave in the bay. Ortiz *et al.* (2000) analyzed analog tide gauge records (Figure 3C) of the Ms7.5 1957 and Ms7.0 1962 earthquakes in an effort to constrain the source areas of those events. However, no significant attention was paid to understanding the hydrodynamics of amplification. For this purpose the 2021 provides an excellent opportunity to analyze the response of the bay and the region to forcing by local events.

Specifically three phenomena are of interest: resonance of the semi-enclosed bay, shelf modes, and edge waves. Oscillations in bays are well understood - tsunami excitations are trapped by the enclosed shoreline and have periods dependent on the shape, dimension, and depth of the bays. This trapping leads to long

duration events with waves of very specific periods (Rabinovich, 2010). For Acapulco we expect behaviors similar to those already identified from far-field events (Ortiz-Huerta et al., 2018). Shelf modes are resonant phenomena as well. Because tsunami wave speeds depend on the square root of depth, abrupt changes in bathymetry are analogous to impedance contrasts in seismology. Tsunami waves can become trapped in the low velocity continental shelf between the coast, which acts like a reflecting boundary, and the deep, high velocity, trench. Edge waves meanwhile are analogous to surface waves in seismology. Trapped by refraction along the “rigid” boundary that is the shoreline, these oscillations travel along strike of the fault and always in the near-shore environment. For regional events shelf modes and edge waves contribute to the protracted duration of hazardous waves and currents (e.g. Yamazaki & Cheung, 2011; Cortes et al., 2018). In Mexico, Melgar & Ruiz-Angulo (2018) previously identified significant contributions from both shelf modes and edge waves to a very long duration (~48 hr) tsunami produced by the 2017 M8.2 Tehuantepec earthquake east of the Acapulco region. There, however, the Gulf of Tehuantepec is extremely flat and broad and ideal for both phenomena to be well-expressed. Meanwhile in the Guerrero region the shelf is very short - the coast gives way almost immediately to the continental slope (Figure 1,2). So, a priori, one would expect a more muted contribution from shelf modes and edge waves.

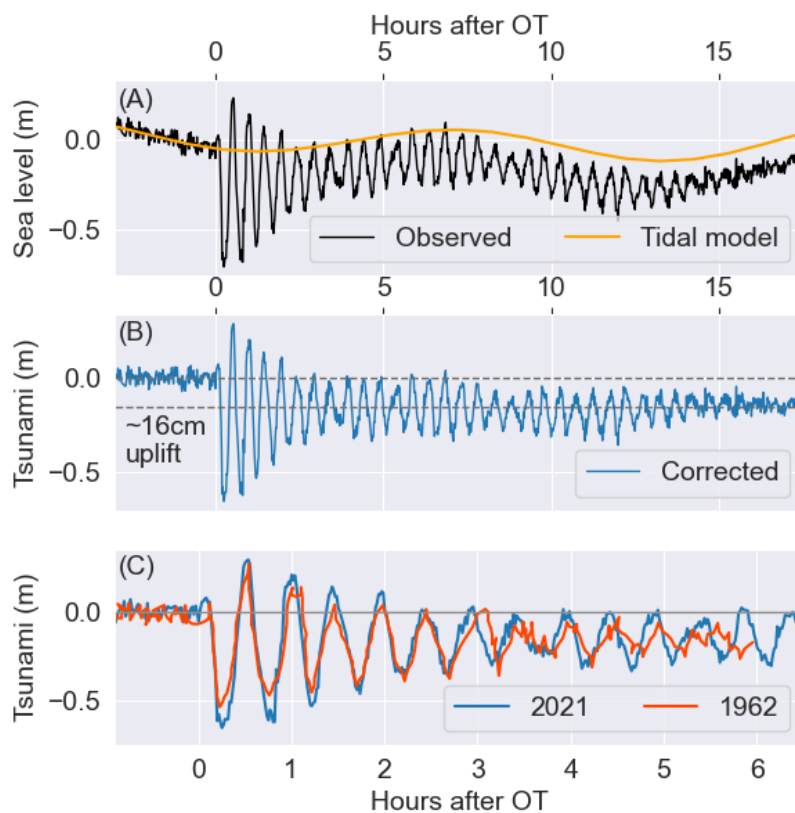


Figure 3. Tsunami observations at the Acapulco tide gauge. (A) Raw observations and tidal model. (B) Tsunami after removing the tides. Dashed lines show a drop in water level corresponding to coseismic uplift of ~16cm. (C) Comparison between the 2021 and 1962 tsunami records.

Within this context we will use the earthquake source model inverted from regional geophysical data as the initial condition to produce a high resolution hydrodynamic model of the 24 hrs following the onset of the tsunami. The goal is to understand the mechanisms of amplification. We will show, somewhat counter-intuitively, that while simple resonance of the enclosed bay is certainly important, the duration of excitation has a significant contribution from edge-waves and shelf modes. While very short, the continental shelf between -103° and -98° is still capable of producing these two phenomena. They are long lasting, confined to the near-shore region, and continuously feedback into and “re-excite” the bay resonance. If these were absent the duration of the tsunami in the bay would be far shorter. We also find that because the bay (and the coast) undergoes uplift, for the first ~ 30 mins after the onset of the event, the tsunami currents are

directed out of the bay, effectively flushing it, even when tsunami waves are propagating into it. These currents achieve significant speeds in excess of 1 m/s in localized parts of the bay and are potentially quite hazardous (e.g. [Lynett et al., 2014](#)). Finally, we note that the phenomena is of interest beyond the sphere of academic research. The city of Acapulco, which surrounds the bay ([Figure 1B](#)) is home to ~800k people and most of the economic activity of the region is tied in some way to the bay. Deepening the understanding of the physics underpinning the peculiar tsunami hazards of the bay is of fundamental importance towards increasing resilience of the region.

DATA AND METHODS

Geophysical Observations and Processing

In order to produce a model of the slip on the fault we rely on high-rate GNSS, strong motion, InSAR line of sight (LOS) data, and the coseismic offset from the ACAP tide gauge ([Figure 1](#)). For validation of the tsunami model we rely on the time-varying tide gauge recording. Processing applied to each of these is detailed below.

Crustal deformation

We processed InSAR data from ascending track 78 of the Copernicus Sentinel 1 satellites ([Figure 2B](#)). Single interferograms for this track have substantial atmospheric noise that partly obscured the coseismic signal and cause large errors in estimating the coseismic displacements. To ameliorate this, we processed a series of interferograms that span a month and a half before and after the earthquake. Using InSAR time-series analysis ([Yunjun, et al., 2019](#)), we estimated a step function at the time of the earthquake. Prior to inversion a ramp was removed to further correct for any remaining long wavelength biases and the interferogram was down sampled using the QuadTree approach ([Figure 4, Lohman & Simons, 2005](#)).

Seismological

Time-dependent information of the elastic wavefield was used for inversion as recorded by two separate sets of instruments. First, four three-component accelerometers operated by the Instituto de Ingenieria, part of the Universidad Nacional Autónoma de México ([See data and resources](#)), ([Figure 1A,4](#)) were used. These were integrated from acceleration to velocity, decimated with an anti-alias filter from 100Hz to 5Hz, and bandpass filtered between 20 s and 0.4 Hz.

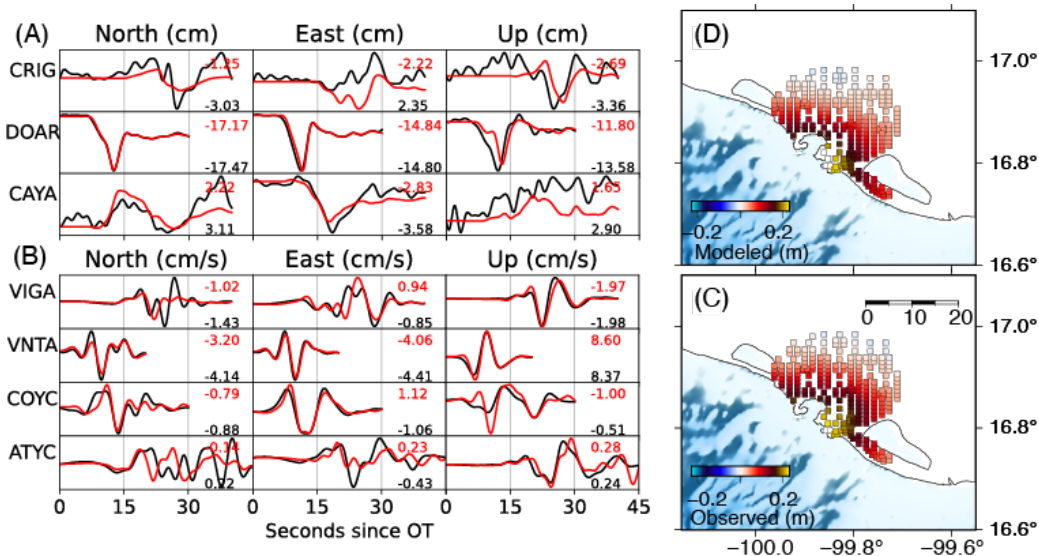


Figure 4. Data fits for the slip inversion. (A) Fits to the HR-GNSS. Red is modeled, black is observed. Numbers indicate the peak amplitudes of each waveform. (B) Same as (A) but for the strong motion data. (C) Down sampled InSAR LOS used in the inversion. (D) Predicted InSAR LOS from the inversion.

Next, three component displacements from three HR-GNSS sites ([Figure 1A,4](#)) were estimated. We use the relative positioning code TRACK ([Herring et al., 2018](#)) with International GNSS Service final clocks and

orbits. Displacements are computed at 5 Hz with respect to station UTON outside Puebla, Mexico. We window the time series such that no ground motion at the reference station will be propagated into the sites used in the inversion. The displacements are then low-pass filtered to 0.5 Hz and inverted without decimation. For inversion the vertical channels were down-weighted by a factor of three to account to the well-known higher noise levels in this direction of motion (e.g. [Melgar et al., 2020](#))

Tsunami

A single tide gauge recording at station ACAP inside Acapulco Bay ([Figure 1B,3](#)) is of critical importance for validating the hydrodynamic model. The device records water levels at 1 minute intervals. We estimated the tide time series at the location of the gauge using the Tide Model Driver package ([Egbert and Erofeeva, 2002](#)), which implements the fully global solution TPX09-atlas ([Figure 3A](#)). The tides were then removed from the record ([Figure 3B](#)) revealing that, in addition to the tsunami there is a coseismic drop of ~16 cm in water level. This is consistent with uplift of the tide gauge relative to the datum of mean sea level. We use this offset in the slip inversion as well. We calculated the background noise level of the sensor using 6 hrs of pre-event noise and estimated the waveform envelope using the Hilbert transform ([Figure 1C](#)). The envelope provides a simple way of measuring the time it takes the record to decay back to its pre-event condition and thus estimate the duration of the tsunami.

Additionally, to analyze the time-frequency behavior of the tsunami observations (and later of the model output) we use the Hilbert-Huang transform (HHT) ([Huang et al., 1998](#); [Huang & Wu, 2008](#)). The HHT relies on empirical mode decomposition of the time series into a user-defined number of intrinsic mode functions (IMFs). These IMFs are themselves time series which are guaranteed, by construction, to contain only a single frequency component at any instant in time. The approach then consists of applying the Hilbert transform to each IMF in order to estimate the instantaneous frequency of each as a function of time. The HHT provides the same information as a spectrogram (frequency content as a function of time), familiar to most geophysicists. Traditionally this has been estimated using Fourier analysis of overlapping windows of the original time series – but, the HHT has the added benefit of much higher precision in the time-localization of when each frequency component occurs. Details of this superior performance over traditional Fourier, and even wavelet techniques, are in [Huang et al. \(1998\)](#). We chose this approach because the slow sampling of the tide gauges and the long period of the tsunami oscillations made it challenging to use traditional Fourier techniques.

Earthquake Source Model Inversion

To invert for the time history of slip, we use the MudPy slip inversion code ([Melgar & Bock, 2015](#)). This is a linearized approach which uses the multi-time window method for estimating the amount of slip and its onset times across the fault. We assume the megathrust geometry from the Slab 2 database of subduction zones ([Hayes et al., 2018](#)). This is very well constrained for the Guerrero region. In addition to being informed by focal mechanisms, here the geometry includes constraints from receiver functions and tomography from dense deployments of temporary networks ([Perez-Campos et al., 2008](#)). The 3D fault geometry is discretized into 256 triangular subfaults ([Figure 1A](#)) using a finite element mesh.

Static and elastodynamic green functions for the InSAR, HR-GNSS, and strong motion data are calculated using the frequency wavenumber approach of [Zhu & Rivera \(2002\)](#). We assume a 1D layered Earth structure obtained by taking a vertical profile at the epicentral region through the 3D model for Mexico of [Spica et al. \(2016\)](#). We allow slip to occur on five 50% overlapping triangle slip rate functions. Each slip rate function has a rise time of 1 s. This value was chosen because it is roughly consistent with what's expected from rise time-magnitude scaling laws derived from worldwide events ([Melgar & Hayes, 2017](#)). We also test several allowable rupture speeds ranging between 2.8 and 4.6 km/s. To nucleate rupture we assume the hypocenter provide by the national network of the Servicio Sismológico Nacional (SSN) which is located at (-99.93°, 16.77°, 13.7 km). This is approximately 20 km southwest of the hypocenter reported by the U.S. Geological Survey (USGS). This is a well-known bias in USGS locations for Mexico (e.g. [Hjorleifsdottir et al., 2016](#)). The inversion is regularized using a minimum-norm, or zeroth-order Tikhonov, approach. We enforce non-negative slip by limiting the possible rake angles to a window between 45° and 135°.

Tsunami Propagation Modeling

We use GeoClaw for modeling tsunami propagation. It solves the non-linear depth-averaged shallow water equations using a finite volume approach (Berger et al., 2011). GeoClaw is widely used and has undergone careful validation (e.g. Arcos & LeVeque, 2015). Bottom friction is enforced using a Manning-type parametrization. In our simulations we held the friction coefficient fixed at 0.025. GeoClaw also has a moving boundary condition at the shoreline which allows cells in the model to transition between wet and dry states and be inundated. We did not study inundation in this work. Numerical convergence is ensured using the Courants-Friedrichs-Lewy (CFL) condition which we held at 0.75 and ran the propagation model for a total of 24 hrs of model time.

GeoClaw uses adaptative mesh refinement (AMR) and allows bathymetry grids of different resolutions to be used depending on the evolution of the tsunami wavefield. This greatly reduces computational time by only refining regions of the model where significant activity is taking place at any point in time. We used six levels of refinement. These range from an outer coarser grid (AMR1) where cells are 5 arcmin (~10 km) in size, down to the highest level (AMR6) where cells are 1 arcsec (~30 m) in size. We use several different resolution combination bathymetry/topography grids, including SRTM30+ for AMR levels 1 and 2, and SRTM15+ for AMR level 3 (Farr et al., 2007; Tozer et al., 2019). For AMR levels 4-6 we combined digital nautical charts purchased from a private company (see Data and Resources) along with the SRTM1 topography-only dataset. These higher resolution grids are only used in the vicinity of the bay (Figure 1B)

In addition to the water level perturbations, η , we also study the horizontal currents, v_h , produced by the tsunami. We also estimate the energy budget for the tsunami E_T which is the sum of the potential and kinetic energies such that

$$E_T = E_P + E_K . \quad (1)$$

The tsunami potential energy, E_P , at a particular point in time is obtained from

$$E_P(t) = \int \int \eta(x, y, t) \rho g \, dx dy, \quad (2)$$

Where ρ is the density of seawater and g the acceleration due to gravity. x and y are the two horizontal coordinates and the integral is taken over the offshore area that experiences perturbations to η . Meanwhile the kinetic energy, E_K , as a function of time can be calculate from

$$E_K(t) = \int \int \rho (v_h[x, y, t])^2 \, dx dy, \quad (3)$$

Where once again, the surface integral is taken only over the offshore region undergoing tsunami perturbations. For the tsunami models we perform this calculation as a function of time analyzing the energy content at each time step.

RESULTS AND DISCUSSION

The Earthquake Source

The final earthquake slip model is shown in Figure 1A. Its seismic moment is $M_0=3.92 \times 10^{19}$ ($M_w 7.0$) and it is characterized by two predominant asperities, one up-dip of the hypocenter with peak slip of 1.5 m and one down-dip of the hypocenter with peak slip of 2.3 m. This leads to two distinct patches of coseismic uplift (Figure 2B), one partly onshore and offshore with a maximum of 20 cm and another further offshore with ~10cm of peak uplift. The bulk of the slip is neatly contained between the 10 and 20 km depth contours. To determine whether these features are well resolved we performed jackknife analysis following the methodology proposed by Kim & Dreger (2008). We randomly removed 20% of the input data into the inversion and reinverted. We replaced the data and removed another random 20%. The process was repeated 200 times. The results are shown in Figure 5. As expected, the mean slip model is nearly identical to the slip in Figure 1A. The standard deviations of slip (Figure 5B) can be used as proxies for uncertainty and are of the order of 0.2-0.5 m for the larger slip asperities. Meanwhile, the coefficient of variation (CV, Figure 5C) which is the ratio of the standard deviation of slip to the mean slip identifies areas that are poorly resolved. A large CV is indicative of portions of the slip model that change wildly in amplitude depending on which data is removed in the jackknifing process. The two main slip asperities have relatively low CVs indicating that they persist and are required by the data.

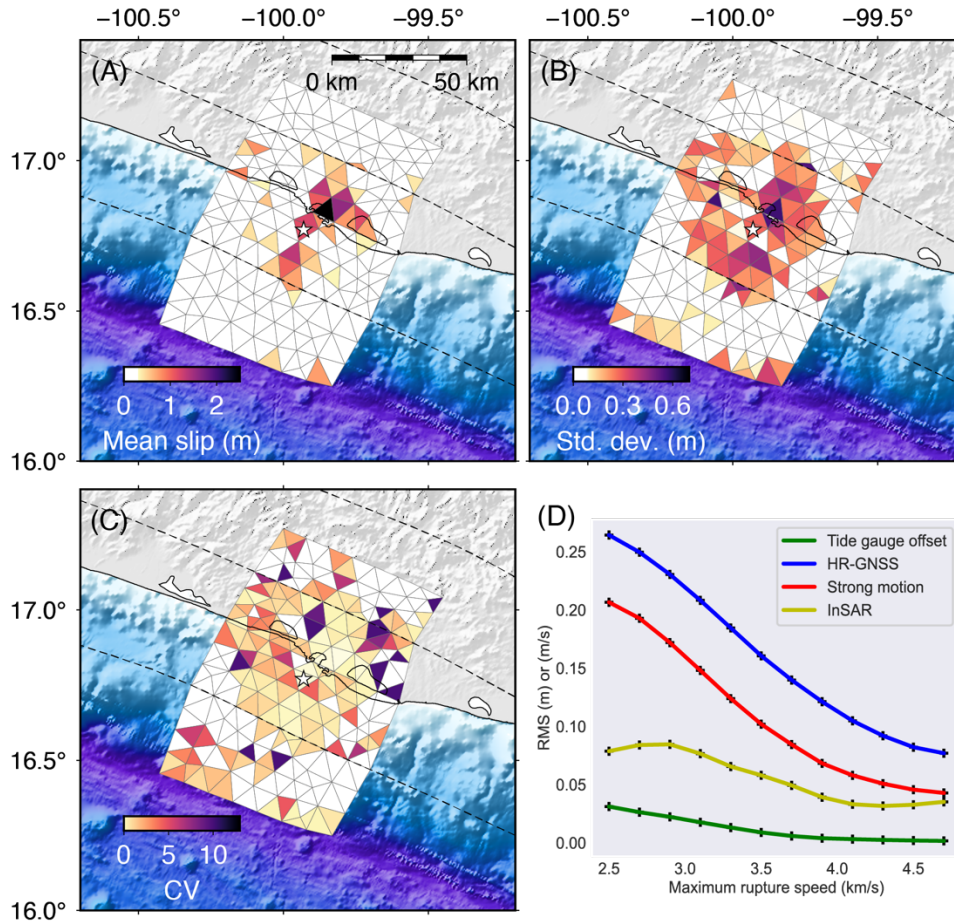


Figure 5. Inversion sensitivity analysis using a jackknife approach after removing with replacement 20% of the data. (A) mean slip model (B) Standard deviation of slip and (C) Coefficient of variation (ratio of mean to standard deviation). (D) Sensitivity of each data type used in the joint inversion to the maximum allowed rupture speed. In all panels the white star is the event hypocenter and dashed lines are the slab depth contours from Hayes et al. (2018) at 10km intervals

The down-dip limit of slip for this event is well constrained thanks to the on-shore InSAR in particular (Figure 2A,4C). It is shallower (~20km) than what is observed in the 1995 M7.3 Copala and 2012 M7.5 Pinotepa earthquakes ~100km to the east. For those events, slip is imaged to extend closer to ~25km in depth (Courbouleux et al., 1997; UNAM Seismology Group, 2013). Whether there is residual deeper slip left to be used in future events is not possible to ascertain at this point. Although geodetic coupling models suggest the potential for this - they image meaningful coupling at least to 25-30 km depths in this region (Rousset et al., 2016, Maubant et al., 2022)

Whether the up-dip limit of slip for the event is reliable is important. It has been shown that, unlike in strictly static inversions, where offshore slip occurs is uniformly difficult to pin down, the use of time-varying data such as HR-GNSS and strong motion data greatly ameliorates this. The pulses of velocity and displacement happen at specific times in the records, those can only originate from certain parts of the assumed rupture geometry and thus serve as strong constraints on offshore slip. A good example of this can be found in the resolution analysis of the 2015 Illapel, Chile earthquake (Melgar et al., 2016). For this reason, and given the jackknife results, we argue that 10 km up-dip limit is likely a real feature.

Indeed, this upper limit of slip this is broadly consistent with large earthquakes in this part of the subduction zone. Immediately due east of this event the 1995 M7.3 Copala, 2012 M7.5 Pinotepa, 2018 M7.2 Ometepac, and 2020 M7.4 La Crucecita earthquakes all have up-dip limits of slip at ~10km (Courbouleux et al., 1997; UNAM Seismology Group, 2013; Li et al., 2018; Melgar et al., 2021). This up-dip limit seems persistent for large M7+ events in the region and the open question remains of whether slip between 10 km

depth and the trench is possible in Mexico. Geodetic coupling models identify at least modest coupling (~ 0.4) at these shallow depths (Maubant et al., 2022), and Singh et al. (2016) also found evidence of near-trench seismicity being depleted in high-frequencies, essentially behaving like small “tsunami earthquakes” (e.g Newman et al. 1998). In aggregate, this suggests that shallow slip is mechanically feasible. However, it is understood that there is room for uncertainty, coupling models, because they are based on on-shore quasi-static observations alone, struggle with imaging offshore. Data from offshore geophysical deployments (Cruz-Atienza et al., 2018) have been analyzed and been used to identify episodic shallow tremor and potentially slow slip events (Plata-Martinez et al., 2021). Yet, full characterization of mechanical coupling remains elusive. The question is of fundamental importance for tsunami hazards - geologic evidence of tsunami deposits up to ~ 5 km inland produced by the 1787 M8.6 San Sixto earthquake (Ramirez-Herrera et al., 2020) immediately east of the 2021 source region suggest that during extremely large events shallow slip is certainly a possibility.

Spatially the event is quite compact and the same is true from a kinematic standpoint. It is short in duration (~ 18 s) and the data themselves prefer a fast rupture velocity. This can be seen in Figure 5D, a maximum velocity of ~ 4 km/s produces the lowest root mean square (RMS) misfits to the data. At the depths where the majority of slip occurs the 3D velocity model (Spica et al. 2016) has shear wave speeds of 3.7-4.0 km/s. We note that in the multi-time window slip inversion approach we have used here this rupture speed is the *maximum allowed*. Slower propagation is permitted and would be reflected by meaningful moment release in later time windows. As a result, the rupture velocity results of Figure 5D do not necessarily imply that rupture is super-shear, although they do suggest strongly that it is fast, likely propagating close to local shear-wave speeds. In this analysis we varied the allowed maximum rupture speed and considered the RMS misfits to all of the data types used in the inversion. Evidently, static data, such as InSAR has no intrinsic sensitivity to kinematics. However, as the time-varying data (HR-GNSS and strong motion) accommodate the changes in rupture speed this impacts the quality of the fits to the static data as well. For this reason we prefer to analyze the impact of varying rupture speeds to all data types simultaneously rather than by inverting them independently.

Within a broader context it is interesting that the 2021 earthquake ruptures very close to, or in the same source region, as a doublet of events that occurred in 1962. Two earthquakes with magnitudes $M_s 6.7$ and $M_s 7.0$ occurred within 7 days of each other (Figure 1A). We digitized the analog mareogram from the larger event (Ortiz et al., 2000) recorded at the same site within Acapulco Bay (Figure 1C) and de-tided it using the same procedure as that for the 2021 record. The two recordings are strikingly similar. The onsets of the first perturbations are almost identical, and, while we only have the first 6 hrs for the 1962 recording, it is apparent that its coseismic offsets is also very similar. As we will show in the next section, the bay acts essentially as a filter for tsunami energy, preferring to resonate at a very specific period (~ 30 min) irrespective of the source. As a result any tsunami occurring within it will likely always have a very similar behavior. So, it is hard to ascertain from this comparison alone that the 2021 earthquake is a repeat of 1962, however, the suggestion is there, and the prospect of it is tantalizing.

Analysis of Tsunami Behavior in the Bay

Since the ACAP tide gauge is the only hydrodynamic observation of the event within the bay, to validate the model, it is important to match it well. Figure 6A shows very good fits between the model and the observation for the first ~ 6 hrs after origin time (OT). Afterwards the waveforms continue to be very similar but a phase shift begins to manifest – the modeled waveform shows a slight delay and by ~ 12 hrs the waveforms are offset by about $\frac{1}{4}$ of a wavelength. We only have higher resolution bathymetry for the bay so it is most likely that this delay introduced by imperfect resolution of the bathymetry outside it introducing artificial delays (e.g Romano et al., 2015). Nonetheless the waveforms shapes are a close match, and their temporal evolutions otherwise similar, as noted by the waveform envelopes (Figure 6B). The tsunami is observed above the noise in the envelopes up to ~ 15 hrs after OT.

Their data and model agree very well in the frequency domain as well (Figure 6C,D). The observations have a narrow spectral peak in the ~ 20 -40 min period range, with most of the energy split into two sub-peaks at ~ 29 and 32 mins. The model captures this, albeit with slightly less power. One area of divergence is at short periods, here, the model has slightly elevated spectral content at ~ 5 -10 min periods which is not seen in the observations. The spectrograms for the observations (Figure 6C) suggest that there is noise potentially obscuring this.

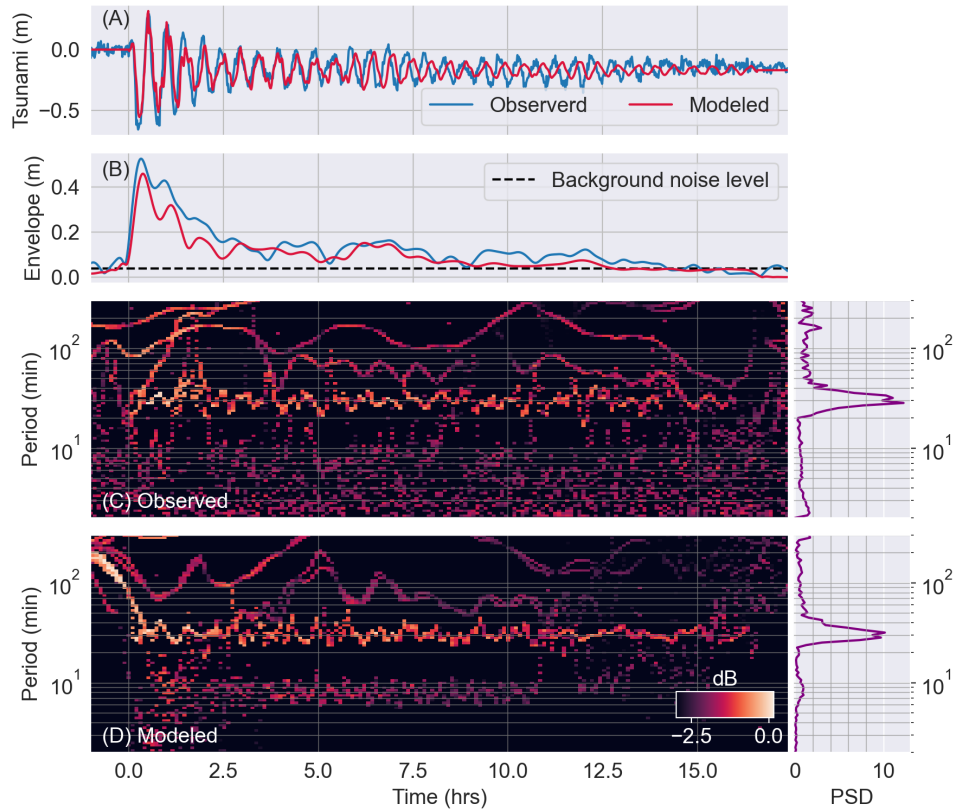


Figure 6. (A) Comparison between observed and modeled tide gauge records inside Acapulco Bay. (B) Comparison of observed and modeled waveform envelopes constructed from the Hilber transform of each. (C) Spectrogram of the observed data and integrated amplitude spectrum constructed using the empirical mode decomposition approach (D) Same as (C) but for the modeled tsunami record.

The above discussion suggests that the hydrodynamic model is very reliable, at a minimum inside Acapulco bay, and captures many of the details of the tsunami. Figure 7 shows the snapshots of the hydrodynamic model that feature the resonant behavior of the bay in the first hour after origin time. The ~30 min period of oscillation is clear, albeit with some interesting complexities. For example, the interactions between the main part of the bay and the smaller Puerto Marquez bay to its southeast is such that each of these resonates out of phase with the other. This is also clear in Figure 8A where we have plotted the dominant period of the tsunami and the differences in the oscillation frequencies of the two bays are clear.

Also of note is that for the first ~15 minutes the tsunami currents (Figure 7) are directed out of the bay, even when the tsunami waves are inbound to it. Recall that the entire bay is uplifted by ~15-20 cm (Figure 2B), so, this initial stage of the tsunami reflects the uplifted waters of the bay being flushed out as the water levels relax down to mean sea level. Indeed the currents can be quite strong. Figure 8B shows the maximum current observed for the full 24 hrs of propagation time. These peak in some regions in excess of 1 m/s. Although it is not until currents reach 3-6 m/s that significant damages are expected, currents like the ones in Figure 8B while, still modest, begin to enter the range where they are considered hazardous to infrastructure (Lynett et al., 2014).

The nature of amplification: bay resonance, shelf modes, and edge waves

Long duration oscillations and hazardous currents are to be expected. After all, Acapulco is an enclosed bay. However, the nature of the long duration of the event is not as straightforward as simple resonant phenomena. Numerical experiments of tsunami amplification of bays in Alaska and New Zealand led Belloti et al. (2012) to conclude that shelf modes and edge waves contributed to amplification by continuously re-exciting the bay resonance. We find that to be particularly true for Acapulco – consider Figure 9 where we

show snapshots of tsunami propagation for the first 6 hrs and for ~700 km of coast along-strike of the trench. The continental shelf in this part of Mexico is both steep and short. These conditions are not favorable for development of shelf-modes and trapping of edge waves (e.g. Geist, 2013). Nonetheless the modest shelf between -103° and -98° still manages to trap waves and we see vigorous tsunami activity between the coast and the 1000 m depth contour. It stands to reason then, that when the edge waves in particular, traverse the entrance to the bay they re-excite the resonance, in effect injecting new energy and re-invigorating the tsunami in the bay.

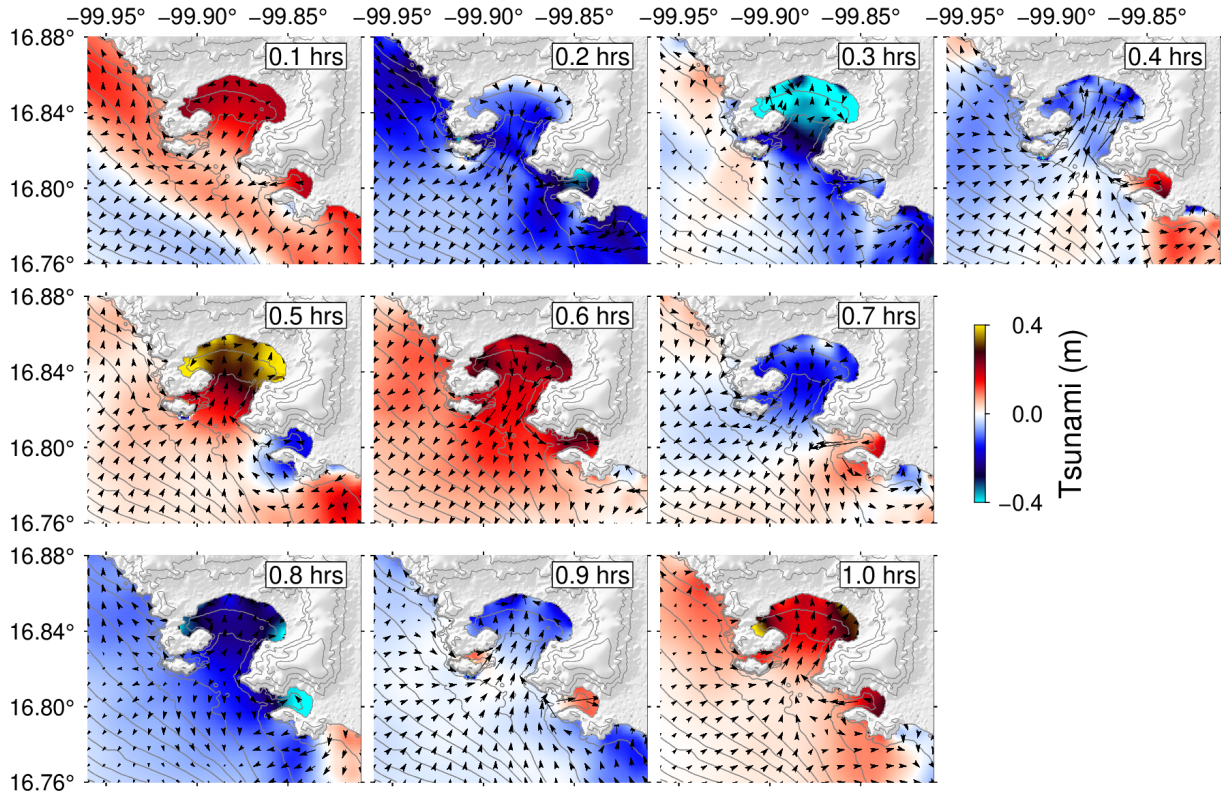


Figure 7. Snapshots at 6 min intervals of tsunami propagation inside Acapulco bay for the first hour after origin time. The colors denote the sea surface elevation while the arrows denote the direction of the tsunami current. Grey contours are bathymetry at 20 m intervals and topography at 100 m intervals

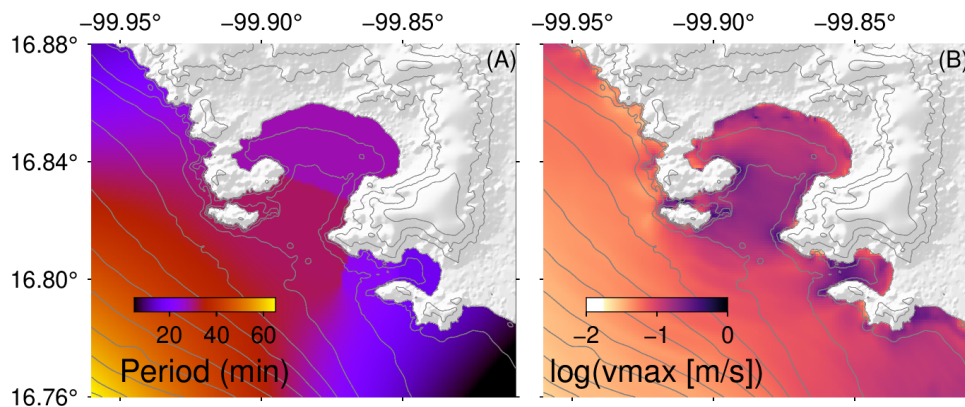


Figure 8. (A) Predominant period of the tsunami oscillations for the full model propagation time defined as the largest amplitude peak in the spectra. (B) Maximum current observed in the model. Grey contours are bathymetry at 20 m intervals and topography at 100 m intervals

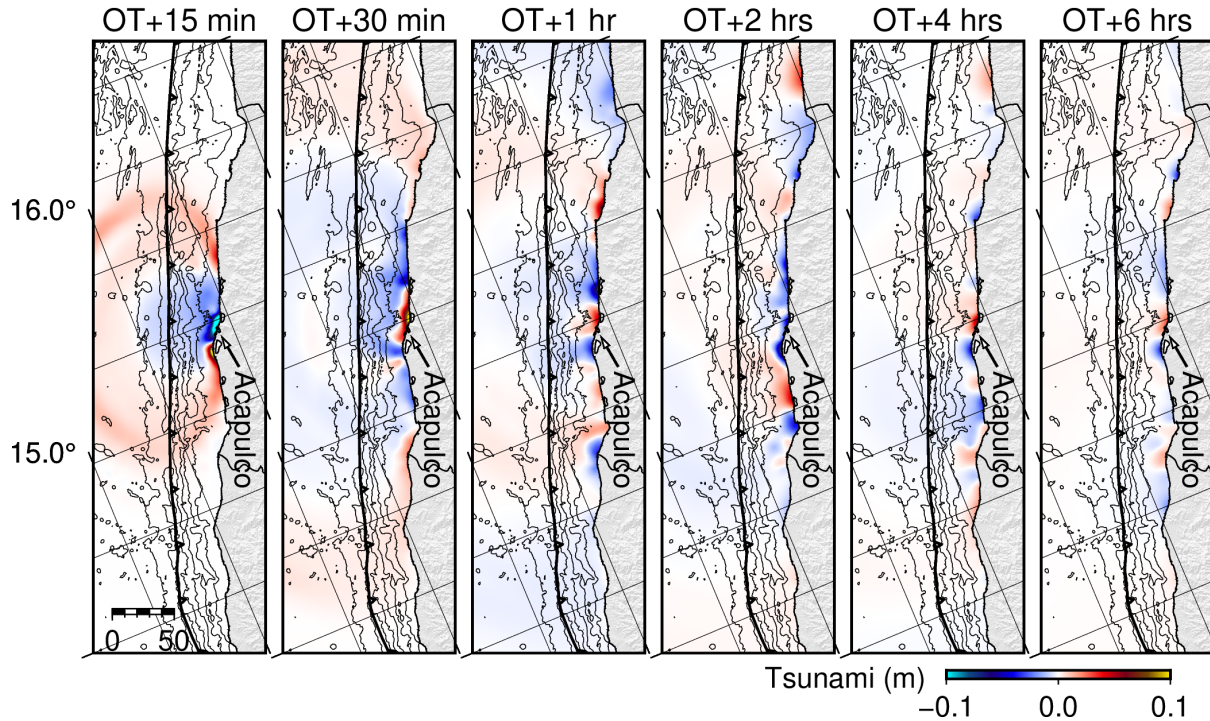


Figure 9. Oblique view and snapshots of edge waves trapped in the continental shelf. Bathymetry is shown at 1000 m contours. The barbed line is the Middle America Trench.

To test this idea we ran a second tsunami model using the same initial condition but with an added restriction. We set up the mesh refinement conditions such that all areas *outside* of the bay were restricted from any refinement. In practice, this means that only very coarse resolution bathymetry is allowed everywhere outside the bay, while within the bay the full resolution bathymetry is used. The effect of this is to numerically dampen, and almost altogether discourage, the formation of shelf modes and edge waves while still allowing the bay resonance to occur as before. Figure 10A shows the results of this at the ACAP tide gauge. Here we can see that, for the model with no edge waves or shelf modes, the amplitude decay after the first maximum is near-monotonic and like a decaying exponential. This is what would be expected for a dampened resonator such as a bay. Meanwhile in the full model, where the bay resonance occurs alongside shelf modes and edge waves, the oscillations last many more hours and have a more complex decay behavior. The period of the main oscillation is identical (~30 min, Figure 10B) but it is clear that there is a lot of spectral content missing from the model with no edge waves or shelf modes. A better view of this is in Figure 10C, here we calculated the tsunami energy as a function of time integrated over the entire bay using EQs1-3. For the first ~4hrs the decays are similar, but after that, the model with no edge waves or shelf modes remains well over half an order of magnitude smaller, in terms of energy content, than the full model. In fact, one can see energy peaks at ~6 and ~12 hrs in the full model where the tsunami is re-energized most likely as a result of edge waves travelling along the shelf (Figure 9).

CONCLUSIONS

The earthquake source

The 2021 M7 Acapulco earthquake occurred within the Guerrero gap, a region long identified as a source of concern for its seismic potential. It had a very compact rupture, between 10 and 20 km depth, with two predominant asperities. The slip model shows that there is plenty of megathrust left to break. There is debate as to whether all of the gap is seismogenic, as there is evidenced of reduced geodetic coupling (Maubant et al., 2022). Nonetheless, there have been numerous past events in this portion of the margin (Suarez et al., 2020), but, whether the 2021 Acapulco earthquake signals a reactivation of the gap since the last period of activity in 1962 (Ortiz et al., 2000), remains to be seen. Of note, the tsunami records

between the 1962 and 2021 events are nearly identical. Interpretation of this fact is complicated by the amplification effects of the bay, but this can be taken as weak evidence that 2021 is a repeat of, or at least very similar, to the 1962 earthquake. It is also interesting that the up-dip limit of the event (~ 10 km) is consistent with what has been seen in slip models of other large earthquakes of the last 30 years. While there are paleoseismic reasons for believing co-seismic slip shallower than this is possible in Mexico, this has not yet been seen in a contemporaneous megathrust event.

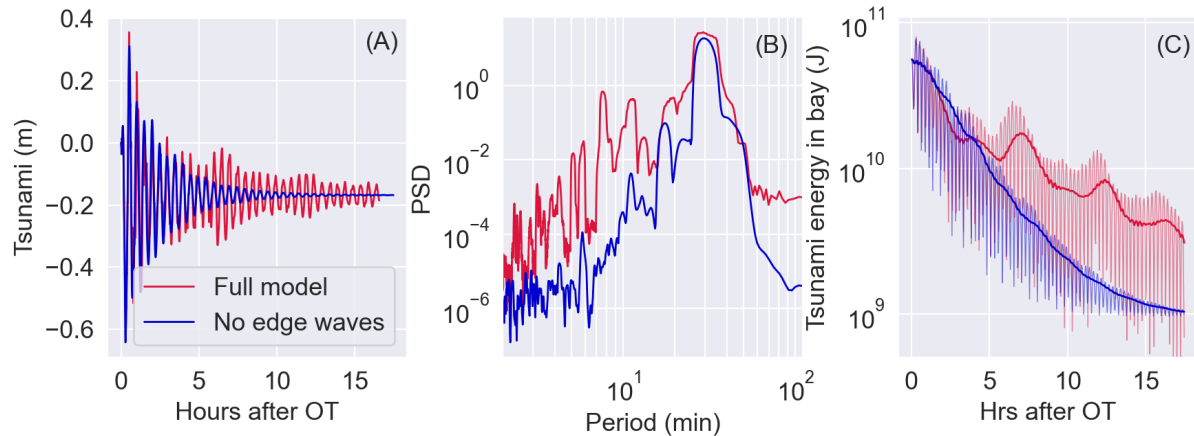


Figure 10. (A) Synthetic records at the ACAP tide gauge. Comparison between the model with full resolution bathymetry versus the model with low resolution bathymetry outside of the bay which precludes edge wave trapping. (B) Power spectra for the waveforms in (A). (C) Temporal evolution of tsunami energy integrated over all of the inside of Acapulco Bay for both models. Thin lines are the 30 s sampled results, thick line is the 30 min. moving average.

Tsunami behavior and hazards

The tsunami had a protracted duration (~ 15 hrs). This was at first blush, unsurprising, given the shape of the bay and its known ability to act as a resonator, trapping, and amplifying tsunami energy. However, a detailed analysis of the hydrodynamic model reveals that the bay alone is not responsible for the long duration of the event. Edge waves and shelf modes, which represent tsunami energy trapped in the near-shore environment, are, somewhat surprisingly, expressed well in the short shelf offshore Guerrero. These two phenomena also produce long duration oscillations lasting many hours, and, as a result, continuously reinvigorate the bay resonance. It is the interplay between these three phenomena that is the mechanism responsible for Acapulco Bay's peculiar amplification characteristics. The hydrodynamic model also revealed that currents can be quite meaningful, even when water level disturbances are modest. For hazards, this suggests that when considering long-term assessments in probabilistic frameworks for the region (e.g. [Salazar-Monroy et al., 2021](#)) it is important to include long-duration modeling, and a wide aperture geographic domain to allow these features to be expressed in the numerical model. Further we stress that amplitudes alone are insufficient to characterize the full extent of the tsunami threat in the region, currents, and duration of disturbances must be quantified as well.

ACKNOWLEDGMENTS

This research was partially funded by NASA grants 80NSSC19K0360 and 80NSSC19K1104. We'd like to thank Zack Spica and Mathieu Perton for their help with extracting the velocity profile from the 3D model and Xyoli Pérez-Campos for discussions. We are also indebted to Randy LeVeque and Lloyce Adams for helpful conversations regarding GeoClaw setup. We also thank Victor Hugo Castro, Ivan Rodriguez, Leonardo Guzmán, Citlali Perez, and Arturo Iglesias for their assistance with data access. We thank the European Space Agency for access to the Sentinel-1 data. SSN data products station maintenance, data acquisition and distribution are thanks to its personnel. We extend our gratitude as well to the Instituto de Ingeniería at UNAM for access to the strong motion data and to the Servicio Mareográfico Nacional for access to the ACAP tide gauge.

DECLARATION OF COMPETING INTERESTS

None

DATA AND RESOURCES

All the data and modeling codes in this paper are openly available. The processed data, inversion parameter files, fault model, velocity model, tsunami initial condition, bathymetry files, GeoClaw parameter files, inversion results, and other ancillary files are archived on Zenodo at (<https://zenodo.org/record/6600058>). The slip inversion code MudPy, can be obtained from <https://github.com/dmelgarm/mudpy>. The tsunami modeling code can be obtained from <http://www.clawpack.org/>. Raw strong motion data can be obtained from the Instituto de Ingenieria, UNAM at <https://aplicaciones.iingen.unam.mx/AcelerogramasRSM/Registro.aspx>, raw tide gauge records can be downloaded from the Intergovernmental Oceanographic Commission (IOC) at <https://www.ioc-sealevelmonitoring.org/>. Access to the Sentinel-1 data is available through the ESA portal (<https://sentinel.esa.int/web/sentinel/sentinel-data-access>). Hypocentral locations for events in Mexico can be found at the SSN's catalog web page (<http://www2.ssn.unam.mx:8080/catalogo/>). Digital nautical charts are part of a compilation produced by the Academia Nacional de Desarrollo e Investigación (<http://www.anide.edu.mx/>) and are also provided at the zenodo link above

REFERENCES

- Arcos, M. E. M., & LeVeque, R. J. (2015). Validating velocities in the GeoClaw tsunami model using observations near Hawaii from the 2011 Tohoku tsunami. *Pure and Applied Geophysics*, 172(3), 849-867.
- Bellotti, G., Briganti, R., & Beltrami, G. M. (2012). The combined role of bay and shelf modes in tsunami amplification along the coast. *J. Geophys. Res: Oceans*, 117(C8).
- Berger, M. J., George, D. L., LeVeque, R. J., & Mandli, K. T. (2011). The GeoClaw software for depth-averaged flows with adaptive refinement. *Advances in Water Resources*, 34(9), 1195-1206.
- Castro, R. R., Pérez-Campos, X., Zúñiga, R., Ramírez-Guzmán, L., Aguirre, J., Husker, A., ... & Sánchez, T. (2016). A review on advances in seismology in Mexico after 30 years from the 1985 earthquake. *Journal of South American Earth Sciences*, 70, 49-54.
- Cortés, P., Catalán, P. A., Aránguiz, R., & Bellotti, G. (2017). Tsunami and shelf resonance on the northern Chile coast. *Journal of Geophysical Research: Oceans*, 122(9), 7364-7379.
- Courboux, F., M. A. Santoyo, J. F. Pacheco, and S. K. Singh (1997). The 14 September 1995 (M = 7.3) Copala, Mexico, earthquake: A source study using teleseismic, regional, and local data, *Bulletin of the Seismological Society of America*, 87(4), 999-1010.
- Cruz-Atienza, V. M., Ito, Y., Kostoglodov, V., Hjörleifsdóttir, V., Iglesias, A., Tago, J. & Kido, M. (2018). A seismogeodetic amphibious network in the Guerrero seismic gap, Mexico. *Seismological Research Letters*, 89(4), 1435-1449.
- Egbert, G.D. and Erofeeva, S.Y., 2002. Efficient inverse modeling of barotropic ocean tides. *Journal of Atmospheric and Oceanic technology*, 19(2), pp.183-204.
- Farr, T. G., Rosen, P. A., Caro, E., Crippen, R., Duren, R., Hensley, S., ... & Alsdorf, D. (2007). The shuttle radar topography mission. *Reviews of geophysics*, 45(2).
- Geist, E. L., & Parsons, T. (2006). Probabilistic analysis of tsunami hazards. *Natural Hazards*, 37(3), 277-314.
- Geist, E. L. (2013). Near-field tsunami edge waves and complex earthquake rupture. *Pure and Applied Geophysics*, 170(9), 1475-1491.
- Hayes, G. P., Moore, G. L., Portner, D. E., Hearne, M., Flamme, H., Furtney, M., & Smoczyk, G. M. (2018). Slab2, a comprehensive subduction zone geometry model. *Science*, 362(6410), 58-61.
- Herring, T. A., King, R. W., Floyd, M. A., & McClusky, S. C. (2018). *GAMIT Reference Manual*, Release 10.7. *Mass. Inst. of Technol.*, Cambridge.

- Hjörleifsdóttir, V., Singh, S. K., & Husker, A. (2016). Differences in epicentral location of Mexican earthquakes between local and global catalogs: An update. *Geofísica internacional*, 55(1), 79-93.
- Huang, N. E., Shen, Z., Long, S. R., Wu, M. C., Shih, H. H., Zheng, Q., ... & Liu, H. H. (1998). The empirical mode decomposition and the Hilbert spectrum for nonlinear and non-stationary time series analysis. *Proceedings of the Royal Society of London. Series A: mathematical, physical and engineering sciences*, 454(1971), 903-995.
- Huang, N. E., & Wu, Z. (2008). A review on Hilbert-Huang transform: Method and its applications to geophysical studies. *Reviews of geophysics*, 46(2).
- Kazachkina, E., Kostoglodov, V., Cotte, N., Walpersdorf, A., Ramirez-Herrera, M. T., Gaidzik, K., ... & Santiago, J. A. (2020). Active 650-km long fault system and Xolapa sliver in southern Mexico. *Frontiers in Earth Science*, 155.
- Kim, A., Dreger, D.S., (2008). Rupture process of the 2004 Parkfield earthquake from near fault seismic waveform and geodetic records, *J. Geophys. Res.*, 113 (B7).10.1029/2007JB005115
- Li, Y., X. Shan, C. Zhu, X. Qiao, L. Zhao, and C. Qu (2020). Geodetic Model of the 2018 M w 7.2 Pinotepa, Mexico, Earthquake Inferred from InSAR and GPS Data, *Bulletin of the Seismological Society of America*, 110(3), 1115-1124.
- Lohman, R. B., & Simons, M. (2005). Some thoughts on the use of InSAR data to constrain models of surface deformation: Noise structure and data downsampling. *Geochemistry, Geophysics, Geosystems*, 6(1).
- Lynett PJ, Borrero J, Son S, Wilson R, Miller K (2014) Assessment of the tsunami-induced current hazard. *Geophys. Res. Lett.*, doi:10.1002/2013GL058680.
- Maubant, L., Radiguet, M., Pathier, E., Doin, M. P., Cotte, N., Kazachkina, E., & Kostoglodov, V. (2022). Interseismic coupling along the Mexican subduction zone seen by InSAR and GNSS. *Earth and Planetary Science Letters*, 586, 117534.
- Melgar, D., & Bock, Y. (2015). Kinematic earthquake source inversion and tsunami runup prediction with regional geophysical data. *Journal of Geophysical Research: Solid Earth*, 120(5), 3324-3349.
- Melgar, D., & Hayes, G. P. (2017). Systematic observations of the slip pulse properties of large earthquake ruptures. *Geophysical Research Letters*, 44(19), 9691-9698.
- Melgar, D., & Ruiz-Angulo, A. (2018). Long-lived tsunami edge waves and shelf resonance from the M8. 2 Tehuantepec earthquake. *Geophysical Research Letters*, 45(22), 12-414.
- Melgar, D., Fan, W., Riquelme, S., Geng, J., Liang, C., Fuentes, M., & Fielding, E. J. (2016). Slip segmentation and slow rupture to the trench during the 2015, Mw8.3 Illapel, Chile earthquake. *Geophysical Research Letters*, 43(3), 961-966.
- Melgar, D., Crowell, B. W., Melbourne, T. I., Szeliga, W., Santillan, M., & Scrivner, C. (2020). Noise characteristics of operational real-time high-rate GNSS positions in a large aperture network. *Journal of Geophysical Research: Solid Earth*, 125(7), e2019JB019197.
- Melgar, D., Ruiz-Angulo, A., Pérez-Campos, X., Crowell, B. W., Xu, X., Cabral-Cano, E., & Rodríguez-Abreu, L. (2021). Energetic rupture and tsunamigenesis during the 2020 Mw 7.4 La Crucecita, Mexico earthquake. *Seismological Research Letters*, 92(1), 140-150.
- Newman, A. V., & Okal, E. A. (1998). Teleseismic estimates of radiated seismic energy: The E/M 0 discriminant for tsunami earthquakes. *Journal of Geophysical Research: Solid Earth*, 103(B11), 26885-26898.
- Ortiz, M., Singh, S. K., Kostoglodov, V., & Pacheco, J. (2000). Source areas of the Acapulco-San Marcos, Mexico earthquakes of 1962 (M 7.1; 7.0) and 1957 (M 7.7), as constrained by tsunami and uplift records. *GEOFISICA INTERNACIONAL-MEXICO-*, 39(4), 337-348.

- Ortiz-Huerta, L. G., Ortiz, M., & García-Gastélum, A. (2018). Far-field tsunami hazard assessment along the Pacific coast of Mexico by historical records and numerical simulation. *Pure and Applied Geophysics*, 175(4), 1305-1323.
- Pérez-Campos, X., Kim, Y., Husker, A., Davis, P. M., Clayton, R. W., Iglesias, A., ... & Gurnis, M. (2008). Horizontal subduction and truncation of the Cocos Plate beneath central Mexico. *Geophysical research letters*, 35(18).
- Plata-Martínez, R., Ide, S., Shinohara, M., Garcia, E. S., Mizuno, N., Dominguez, L. A., . & Ito, Y. (2021). Shallow slow earthquakes to decipher future catastrophic earthquakes in the Guerrero seismic gap. *Nature communications*, 12(1), 1-8.
- Rabinovich, A. B. (2010). Seiches and harbor oscillations. In *Handbook of coastal and ocean engineering* (pp. 193-236).
- Ramírez-Herrera, M. T., Corona, N., Cerny, J., Castillo-Aja, R., Melgar, D., Lagos, M., & Ruiz-Fernández, A. C. (2020). Sand deposits reveal great earthquakes and tsunamis at Mexican Pacific Coast. *Scientific Reports*, 10(1), 1-10.
- Romano, F., Piatanesi, A., Lorito, S., Tolomei, C., Atzori, S., & Murphy, S. (2016). Optimal time alignment of tide-gauge tsunami waveforms in nonlinear inversions: Application to the 2015 Illapel (Chile) earthquake. *Geophysical Research Letters*, 43(21), 11-226.
- Rousset, B., Lasserre, C., Cubas, N., Graham, S., Radiguet, M., DeMets, C., ... & Walpersdorf, A. (2016). Lateral variations of interplate coupling along the Mexican subduction interface: Relationships with long-term morphology and fault zone mechanical properties. *Pure and Applied Geophysics*, 173(10), 3467-3486.
- Salazar-Monroy, E. F., Melgar, D., Jaimes, M. A., & Ramirez-Guzman, L. (2021). Regional Probabilistic Tsunami Hazard Analysis for the Mexican Subduction Zone from Stochastic Slip Models. *Journal of Geophysical Research: Solid Earth*, 126(6), e2020JB020781.
- Sanchez, A. J. and Farreras, S. F.: 1993, Catalog of tsunamis on the western coast of Mexico. World Data Center A for Solid Earth Geophysics Publication SE-50, National Geophysical Data Center, Boulder, Colorado, 79 pp.
- Sawires, R., Santoyo, M. A., Peláez, J. A., & Corona Fernández, R. D. (2019). An updated and unified earthquake catalog from 1787 to 2018 for seismic hazard assessment studies in Mexico. *Scientific data*, 6(1), 1-14.
- Singh, S. K., Arroyo, D., Pérez-Campos, X., Rodríguez, Q., Iglesias, A., & Ortiz, M. (2016). Fast identification of near-trench earthquakes along the Mexican subduction zone based on characteristics of ground motion in Mexico City. *Bulletin of the Seismological Society of America*, 106(5), 2071-2080.
- Spica, Z., Perton, M., Calò, M., Legrand, D., Córdoba-Montiel, F., & Iglesias, A. (2016). 3-D shear wave velocity model of Mexico and South US: bridging seismic networks with ambient noise cross-correlations (C1) and correlation of coda of correlations (C3). *Geophysical Journal International*, 206(3), 1795-1813.
- Suárez, G., Ruiz-Barón, D., Chico-Hernández, C., & Zúñiga, F. R. (2020). Catalog of preinstrumental earthquakes in central Mexico: Epicentral and magnitude estimations based on macroseismic data. *Bulletin of the Seismological Society of America*, 110(6), 3021-3036.
- Tozer, B., Sandwell, D. T., Smith, W. H., Olson, C., Beale, J. R., & Wessel, P. (2019). Global bathymetry and topography at 15 arc sec: SRTM15+. *Earth and Space Science*, 6(10), 1847-1864.
- UNAM Seismology Group (2013). Ometepe-Pinotepa Nacional, Mexico Earthquake of 20 March 2012 (Mw 7.5): A preliminary report, *Geofísica Internacional*, 52(2), 173-196.
- Yamazaki, Y., & Cheung, K. F. (2011). Shelf resonance and impact of near-field tsunami generated by the 2010 Chile earthquake. *Geophysical Research Letters*, 38(12).

- Yunjun, Z., Fattahi, H., & Amelung, F. (2019). Small baseline InSAR time series analysis: Unwrapping error correction and noise reduction. *Computers & Geosciences*, 133, 104331.
- Zaytsev, O., Rabinovich, A. B., & Thomson, R. E. (2016). A comparative analysis of coastal and open-ocean records of the great Chilean tsunamis of 2010, 2014 and 2015 off the coast of Mexico. In *Global Tsunami Science: Past and Future, Volume I* (pp. 4139-4178). Birkhäuser, Cham.
- Zhu, L., & Rivera, L. A. (2002). A note on the dynamic and static displacements from a point source in multilayered media. *Geophysical Journal International*, 148(3), 619-627.

AUTHOR LIST AND ADDRESSES

- Diego Melgar, Department of Earth Sciences, 100 Cascade Hall, University of Oregon, Eugene, Oregon, USA.
- Angel Ruiz-Angulo, Institute of Earth Sciences, University of Iceland, Sturlugata 7, 101 Reykjavík, Iceland.
- Brendan W. Crowell, Department of Earth and Space Sciences, University of Washington, Johnson Hall Rm-070, Box 351310, 4000 15th Avenue NE, Seattle, WA 98195-1310, USA
- Eric J. Fielding, Jet Propulsion Laboratory, 4800 Oak Grove Drive, M/S 300-233, Pasadena, CA 91109, USA
- Erica A. Solano, Universidad del Mar Campus Puerto Angel, Carretera a Zipolite, 70902 Puerto Angel, Oax., Mexico